UNIVERSITY OF CALIFORNIA,
IRVINE

Numerical Simulation of Droplet Impacting on Solid Surface

THESIS

submitted in partial satisfaction of the requirements
for the degree of

MASTER OF SCIENCE

in Chemical Engineering

by

Chuanning Zhao

Thesis Committee:
Assistant Professor Yoonjin Won, Chair
Assistant Professor of Teaching Daniel Knight
Professor Yun Wang

2019

TABLE OF CONTENTS

LIST OF FIGURES

LIST OF TABLES

ACKNOWLEDGMENTS

I would like to express the deepest appreciation to my committee chair, Professor Yoonjin Won, who inspires me to focus on the two-phase flow research area. Not only did she give me crucial suggestions every time when I ran into troubles in my research, but she offered me many important chances to help me go father in my research. Without her guidance and persistent help this thesis would not have been possible.

I would like to appreciate the advice from my committee members, Professor Yun Wang and Professor Daniel Knight, who help me in comprehending the underlying principles in computational fluid dynamics and microscopic intermolecular entanglements which helped me to construct the mathematical models in this thesis.

Additionally, I would also like to thank my colleagues, Bowen Shao and Shuai Hao, for helping me to set up and conduct the droplet impacting experiments and to understand some key questions in computational fluid dynamics. Moreover, thank UCI Won Lab for providing me facilities and environments to help me to fulfill my thesis.

ABSTRACT OF THE THESIS

Numerical Simulation of Droplet Impacting on Solid Surface

By

Chuanning Zhao

Master of Science in Chemical Engineering

University of California, Irvine, 2019

Assistant Professor Yoonjin Won, Chair

The droplet spreading and bouncing patterns on flat solid surfaces are investigated numerically and experimentally in this thesis. Various parameters are considered to study the droplet impacting behaviors including bottom surface contact angle, droplet diameter, droplet impacting velocity, and impact Weber number. According to the droplet impacting test of varying bottom surface contact angle, the theoretical model predicts both the numerical and experimental results of droplet maximum spreading area and droplet contact time with acceptable accuracy. The droplet maximum spreading area is found to be positively correlated with impact velocity and droplet initial diameter. The droplet contact time is found to be the only function of droplet mass and surface tension which will increase as the droplet size increases.

Chapter.1 INTRODUCTION

The processes of droplets impacting on solid surface can be broadly observed in the nature and is strongly relevant to both agricultural and industrial applications, including wetting of dilute polymer solutions, microfabrication and microchannels, coating manufacture, electrostatic painting, spray ink printing, liquid atomization and cleaning, dynamics of liquid fuel droplets in combustion systems, liquid reactants penetrating through the catalyst in a fixed bed reactor, spray cooling to hot surfaces, and many others. Therefore, it is important to understand the underlying physics associated with those applications that can help to accurately and meaningfully set up the numerical boundary conditions in numerical simulations. In consequence, the numerical results can be used to re-guide the operation of experiments in a less time and money consuming way.

1.1 Introduction of Droplet Impacting

Droplet impacting can be generally classified into (1) droplet impact on liquid films, (2) on liquid pools, and (3) on dry solid surfaces. In this thesis, we chiefly focus on the third regime. Considering solid surfaces with different wettability, the droplet impact form can be divided into hydrophilic surface impact and hydrophobic surface impact.

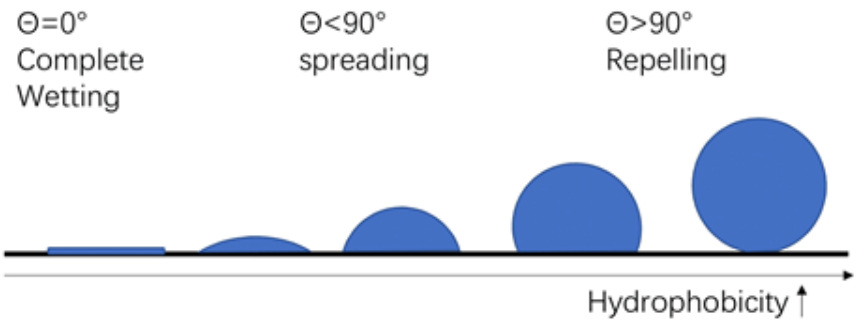

FIGURE1-1. Static droplets sitting on solid surfaces with different wettabilities. From left to right, the wettability decreases and the static contact angle increases.

Solid surfaces with larger wettability always lead to lower mobility for droplet moving and the way of droplet sitting on a structured solid surface is known as the Wenzel state (FIGURE1-2-b). In contrast, it will have a larger tendency for air to be trapped in such complex surface structure while droplet impacting. This least wetting state of solid-liquid interface is Cassie-Baxter (FIGURE1-2-a). However, mostly in real droplet impacting cases, the Cassie-Baxter state is shown in FIGURE1-2-c, and under this circumstance the droplets will have a larger possibility to bounce back. On the contrary, different surface roughness environments such as Wenzel wetting state may lead to disparate outcomes and the droplets will have a large tendency to stick on the surface, accordingly.

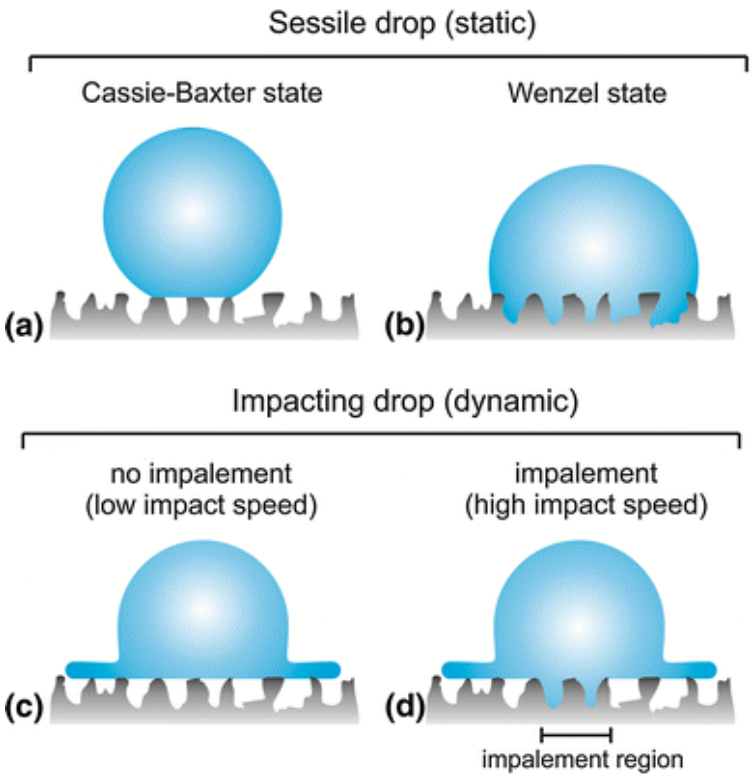

FIGURE1-2. Schematics of the different wetting states on superhydrophobic surfaces, in static and dynamic conditions. A sessile drop on a surface can be in (a) Cassie–Baxter state or in the (b) Wenzel state. When a drop impacts on a superhydrophobic surface:(c)at low impact speed, Cassie–Baxter state is conserved and no impalement is observed, whereas (d) at high impact speed, an area close to the impact zone switches to Wenzel state[1]

After the initial droplet impact moment, the droplet kinetics energy will turn into surface energy and the droplets can splash, spread, and/or bouncing. These diverse outcomes depend on impacting kinetic energy, droplets physical properties, surface incline angle, and surface temperature, etc.

In order to account for all these factors, some important dimensionless numbers are introduced. The most commonly used dimensionless number is Weber number ($We_d \equiv \frac{\rho u^2 d}{\sigma}$), in which ρ and σ are the density (kg/m^3) and the surface tension (N/m) of the liquid,

u and d are the impacting velocity (m/s) and the diameter (m) of the droplet respectively. Weber number represents the ratio of the impacting kinetic energy and the droplet surface energy. While impacting, the contact angle observed at the moving contact line, the dynamic contact angle θ_d, is a function of Capillary number Ca $\equiv \frac{v\mu}{\sigma}$, in which v is the contact-line velocity (m/s) and μ is the liquid dynamic viscosity (kg/m·s). Reynolds number, serving as the ratio of inertial forces over viscous forces, is defined as Re $\equiv \frac{\rho du}{\mu}$. Another important dimensionless number is Ohnesorge number Oh $\equiv \frac{\mu}{\sqrt{\rho\sigma d}} = \frac{\sqrt{We}}{Re}$, which represents the relation of viscous force to inertial force along with the surface tension force.[2]

Under the hydrophobic surface environment, an indispensable property, droplet-solid contact time $t_{contact}$, serves to explain the details of droplet impacting behaviors. Richard [3] found that the droplet-solid contact time is the function of droplet mass m, droplet surface tension σ, droplet density ρ , and impacting velocity v_i. The exact relation is shown below:

$$t_{contact} = 2.6\left(\frac{\rho {d_0}^3}{8\sigma}\right)^{1/2} \quad (1)$$

In reality, droplet impacting velocity tends to have an acute angle with the bottom surface instead of a perfect right angle. Therefore, many experimental and numerical studies will include the inclined surface analysis of droplet impacting on solid surface.

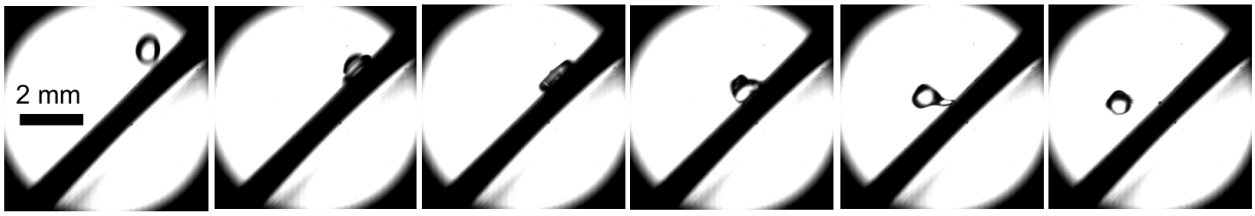

FIGURE1-3. Process of water droplet impacting on an inclined solid hydrophobic surface with the inclined angle equals to 45° .

1.2 Previous Studies about Droplet Impacting

Both of the theoretical and numerical analysis on droplet impacting problem will need boundary conditions sitting at the contact line of three phases as droplets spreading over the solid surface. This is where the wettability (or contact angle) starts to have its influence on droplet impacting process. From Young's equation[4] , the equilibrium contact angle θ_e can be reached from solid-vapor surface tension σ_{sv} and solid-liquid surface tensionσ_{sl}. Directions of these properties are sketched in FIGURE1-4.

$$\sigma \cos\theta_e = \sigma_{sv} - \sigma_{sl} \tag{2}$$

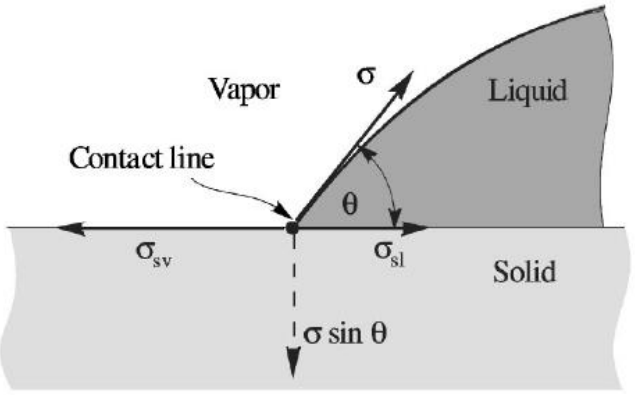

FIGURE1-4. Surface tensions and equilibrium contact angle at a static contact line.[4]

Many previous work have already studied the phenomenon of droplet impacting on dry solid surface. A.L.Yarin et al. [5] reviewed work concerning droplet impacts on thin liquid layers and dry surfaces. The droplet behaviors such as crowns (as shown in FIGURE 1-5) and their propagation, additional kindred and albeit non-splashing were discussed in details along with the phenomenon including droplet spreading, deposition, receding, jetting and rebound. Danial Khojasteh et al. [6] briefly reviewed the possible applications of superhydrophobic surfaces by thoroughly focusing on the most recent advances concerning dynamic droplets impinging the superhydrophobic substrates. Marco Marengo et al.[7] reviewed droplets impacting onto surfaces of higher complexity in morphological way or in chemical way. By introducing morphological changes to the surfaces, the droplet impacts under different surface wettability scenarios are discussed.

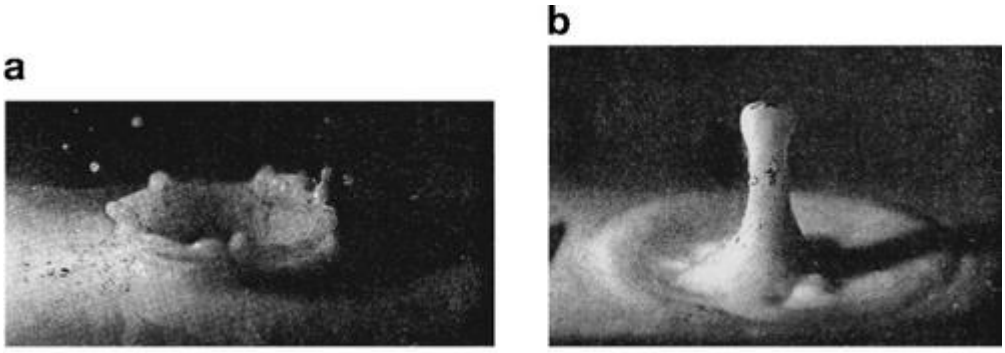

FIGURE1-5. Water drop impact on a deep pool of milk mixed with water. (a) Crater surrounded by a crown-like ejecta at 40ms after the impact. (b) Worthington jet rising from the collapsing crater at 116ms.[48]

In experimental studies, generally, people will use high speed camera to capture the transient process while droplet impacting.

Sani LeClear et al. [8] introduced a series of Weber numbers and discussed how these combinations of different Weber numbers can affect certain dynamics behavior of droplets impinging on inclined superhydrophobic surfaces. They concluded that the Weber numbers based on normal and tangential velocity respectively are in charge of the deformation degree and the other two Weber numbers described by characteristics length **a** of the textured surface are in charge of determining the transition from Cassie-Baxter regime to Wenzel regime.

T Michel et al. [9] experimentally studied the liquid drop impact onto chemically structured surfaces and then obtained the time of droplets spreading on the surface along with the temporal developments of macroscopic dynamic contact angles. The theoretical model they proposed have the ability to predict the experimental data of drop edges evolution as a function of time with great accuracy. This theoretical model involved internal effects, capillary and viscous forces and the dynamic contact angles.

Aiming to understand the droplet impact dynamics and conditions for droplet bouncing on hydrophobic surfaces, Antonini [10] experimentally explored the water droplets obliquely impact onto low wetting surfaces with Weber number ranging from 25 to 585. Their results showed that surface inclining helps to enhance the droplet bouncing and self-cleaning ability by reducing droplet-surface interaction time up to 40%. Moreover, this inclination made droplet bouncing occur even when a certain degree of wetting phenomenon existed on the impacting region.

Jin et al.[11] experimentally investigated the influences of droplet size and surface temperature on the impacting, freezing and melting processes of water droplets impacting on inclined cold surfaces. Their results showed that spreading time, maximum spreading diameter, maximum displacement from the foremost point are all positively correlated to droplet size. Moreover, decreasing the surface temperature resulted in a smoother decreasing spreading factor and a longer retracted distance.

M. Pasandideh-Fard [12]studied the impact of water droplets on a flat solid surface via both experimental and numerical approaches. Varying liquid-solid contact angle by adding traces of surfactant to water, the droplet impact process was captured and their behaviors were measured from photographs. Additionally, as to the numerical analysis part in this paper, they harnessed a modified SOLA-VOF method to model the droplet deformation. The measured values of dynamics contact angle in the experiments mentioned above were used as the boundary condition for this numerical model.

Longquan Chen[13] compared the impact dynamics of water droplets on an artificial dual-scaled superhydrophobic surface to that of a lotus leaf with impacting velocity up to 3 m/s. Different patterns of droplets deformation behaviors were observed for different impacting velocities.

In numerical studies, there are many different computational methods can be applied to the droplet impacting phenomenon.

Llias Malgarinos [14] applied a novel numerical implementation for the adhesion of liquid droplets impacting on dry solid surfaces. This new approach started from the advancing and receding equilibrium contact angles and derived the dynamics contact angle implicitly from the interface shape and the adhesion physics of the gas-liquid-solid interface. And then these dynamic contact angles were required in order to define he wetting properties of liquid phases when interacting with a solid surface.

Yang [15] applied the smoothed particle hydrodynamics (SPH) method and the Peng-Robinson equation of state [16] to describe the two-phase fluid flow with phase change between them. Liu [17] employed the numerical method of volume of fluid (VOF) to simulate the droplet impacting process on computational modeled surface imitating the Canna leaves. Dupont [18] implemented a “sub-grid” description to the moving contact line which is finely valid for some well controlled bi-dimensional situations.

Dashu Li et al. [19] investigated the dynamics and heat transfer of droplet impacting on an inclined wet surface by a numerical model based on coupled level set and volume of fraction (CLSVOF) method. Their numerical results showed the deformation of droplets will spread, form edge jets and splash (as shown in FIGURE 1-6)..

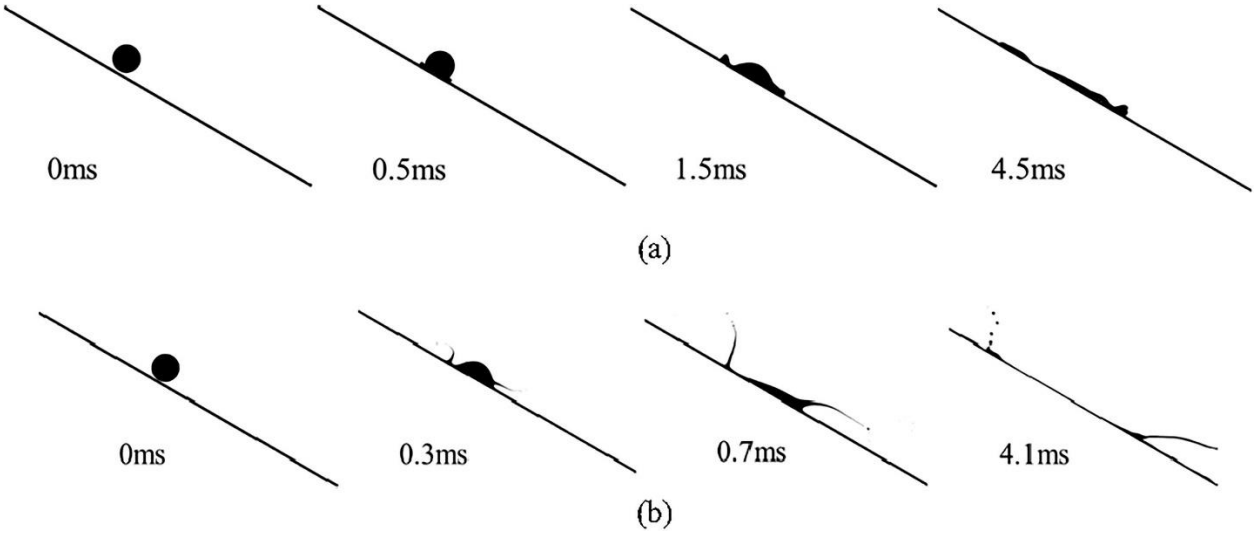

FIGURE1-6. Morphology of droplet impact on wetted incline surface at different impact velocity, (a)1 m/s, (b)6 m/s. Asymmetric thin jets are observed at the front and back spreading edge upon droplet impact due to the effect of the impact angle.[19]

Yang Zhu[20] performed a numerical investigation of drop impact onto a sphere under moderate Reynolds and Weber numbers. The aspect ratio of the sphere to the drop served as the main influence factor of drop spreading and retraction on the sphere and the ratio was quantitatively assessed in this study. Alireza Bordbar et al.[21] applied numerical approach in investigating the spreading and rebound patterns of low-viscous droplets upon impacting spherical solid surfaces. Parameters including impact Weber number, the size ratio of the droplet to the solid surface and the surface contact angle were varied to study their effects on the post-impingement behaviors.

1.3 Problem Description

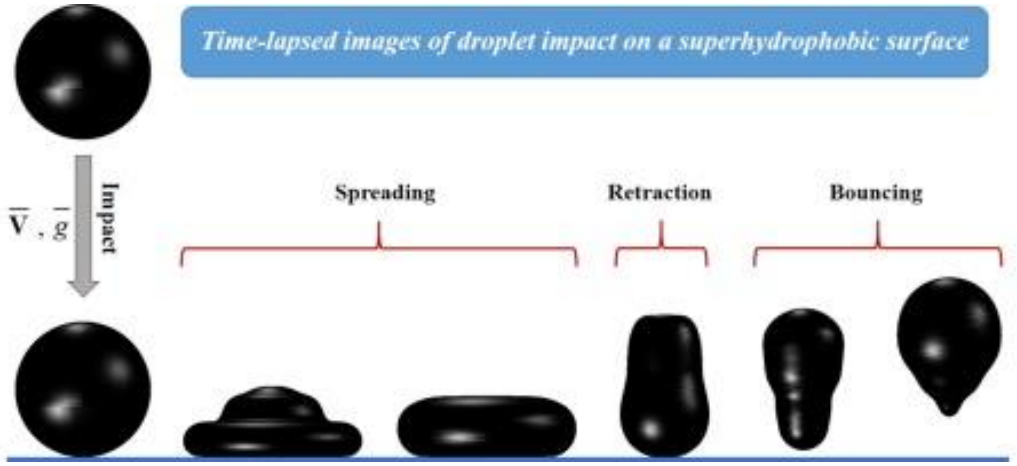

FIGURE1-7. Time-lapsed images of droplet impact on a superhydrophobic surface.[6]

FIGURE 1-7 shows the main steps of droplet impacting on superhydrophobic surface. Generally, the droplet will spread, retract and finally bounce back. While impacting, the droplet will deform and convert its kinetic energy into surface energy and then viscous dissipation will occur sequentially.

The outcome of drop impact varies with impacting velocity, droplet initial size, liquid properties, surface-liquid interfacial tension and surface roughness. Some important parameters that can govern these droplet deformation behaviors while impacting are the initial droplet diameter d_0, the surface inclined angle is α and the initial patched velocity v_0 and impacting velocity v_i. Impacting velocity defines as the drop velocity at the first moment of droplet touching the solid surface.

Chapter.2 METHODS

The mathematical methods and its numerical discretization methods are discussed in this section.

2.1 Mathematical Methods

A VOF (Volume of Fluid) method is used to process the droplet impacting phenomenon. The VOF method qualifies in solving two or more immiscible fluids and is well constructed for two-phase flow. Since the liquid and gas phase will not interpenetrate greatly in this particular case, VOF method is capable for simulating the droplet impacting on solid surface. In this specific case, the air is set to be the primary phase and the secondary phase is water. The properties of these two working fluids are listed in Table 2-1.

Table 2-1. Physical properties of working fluids.

	Density (kg/m^3)	Specific Heat (J/kg·K)	Thermal Conductivity (W/m·K)	Viscosity (kg/m·s)	Surface Tension (N/m)
water	960	4182	0.6	0.001003	0.07199
air	1.225	1006.43	0.0242	1.7894e-05	

The deformation behaviors of droplet impacting are visually shown by phase volume fraction. To track this two-phase interface, in VOF method the continuity equation for the volume fraction of two phases are solved. In the secondary phase, the mass conservation governing equation is shown as

$$\frac{1}{\rho_2}\left[\frac{\partial}{\partial t}(\alpha_2\rho_2) + \nabla\cdot(\alpha_2\rho_2\vec{v}_2)\right] = S_{\alpha_2} + \dot{m}_{12} - \dot{m}_{21} \quad (3)$$

where $\dot{m}_{12}$ is the mass transfer rate (kg/m^2·s) from the primary phase to the secondary phase and the $\dot{m}_{21}$ is the mass transfer rate from the secondary phase to the primary phase. In the droplet impacting process, no additional source term exists, so by default the source term on the right- hand side of Eq.3, S_{α_2}, is zero.

The volume fraction equation above will not be solved for the primary phase, the primirary phase volume fraction will be computed based on the constraint

$$\alpha_1 + \alpha_2 = 1 \tag{4}$$

where α_q represents the volume fraction of each phase.

By choosing the first order implicit scheme for time discretization of the mass conservation equation for the secondary phase, the face fluxes for all cells are obtained by the discretized equation below.

$$\frac{\alpha_2^{n+1}\rho_2^{n+1} - \alpha_2^n \rho_2^n}{\Delta t} + \sum_f \left(\rho_2^{n+1} U_f^{n+1} \alpha_{2,f}^{n+1}\right) = \left[S_{\alpha_2} + \dot{m}_{12} - \dot{m}_{21}\right] V \tag{5}$$

For implicit scheme, the equation above requires the values of volume fraction at the current time step, in consequence this standard scalar transport equation for the secondary phase will be solved iteratively at every time step.

VOF method couples the set of momentum equations along with the energy equation for each phase respectively and the material properties are volume fraction averaged properties. The averaged material properties in this two-phase system are calculated in the form below.

$$\rho = \alpha_2\rho_2 + (1-\alpha_2)\rho_1 \quad (6)$$

$$\upsilon = \alpha_2\upsilon_2 + (1-\alpha_2)\rho_1 \quad (7)$$

Other properties such as thermal conductivity and internal energy are averaged under the similar form.

$$\varphi = \frac{\alpha_1\rho_1\varphi_1+\alpha_2\rho_2\varphi_2}{\alpha_1\rho_1+\alpha_2\rho_2} \quad (8)$$

in which, φ represents all the material properties mentioned above.

The form of momentum and energy conservation equations are shown below.

$$\frac{\partial(\rho\vec{u})}{\partial t} + \nabla\cdot(\rho\vec{u}\vec{u}) = \nabla P + \nabla[\mu(\nabla\vec{u} + \nabla\vec{u}^T)] + \rho\vec{g} + \vec{F} \quad (9)$$

$$\frac{\partial(\rho E)}{\partial t} + \nabla\cdot[\vec{u}(\rho E + P)] = \nabla\cdot\left(k_{eff}\nabla T\right) + S_h \quad (10)$$

in which, k_{eff} serves as the effective thermal conductivity, and S_h refers to the energy source term. Similarly, in this specific case, no extra energy source terms are added to this two-phase system. By default, S_h equals to zero.

Surface tension plays an important role in controlling the transient deformation behaviors within the droplet impacting process. In FLUENT, a continuum surface force (CSF) model is used to transfer surface tension forces into body forces [39]. In this model, the surface tension forces will result in a source term in the momentum equation. Surface curvature is obtained from local gradients along the surface normal direction of the interface. Here, the surface normal is expressed as $\vec{n}$. Then,

$$\vec{n} = \nabla\alpha_2 \quad (11)$$

The interface curvature κ is defined as the divergence of the unit normal $\hat{n} = \frac{\vec{n}}{|\vec{n}|}$.

$$\kappa = \nabla \cdot \hat{n} \tag{12}$$

Using the divergence theorem, the surface tension forces in two-phase flow can be expressed as a volume force in terms of pressure jump across the surface.

$$F_{vol} = \sigma_{12} \frac{\rho \kappa_1 \nabla \alpha_1}{\frac{1}{2}(\rho_1 + \rho_2)} \tag{13}$$

where the ρ is volume-averaged density.

2.2 Numerical Algorithm

From previous discussion, we know that the governing equations are non-linear and coupled which means there must be a certain amount of iterations before the numerical solution converges to an accurate solution in a specific time step. Every procedure within one iteration is given below:

1. Update the flow properties by initialization or the solution from the previous step.
2. Solve the mass, momentum and energy equations simultaneously.
3. Solve the scalar equation of volume fraction using the updated variables from the last step.
4. Check the convergence of all equations.

Once the numerical residual reaches the convergence criteria, stop repeating iterations in current time step and start the iterations for next time step.

To linearize these non-linear momentum conservation equations in every element cells of the flow domain, I choose the implicit method in which the unknown variables in every element cell are obtained through both known and unknown values from their adjacent cells.

The algorithm in dealing with pressure-velocity coupling is SIMPLE (Semi-Implicit Method for Pressure-Linked Equations). SIMPLE algorithm bases on the relation between velocity and pressure corrections to constrain the mass conservation into convergence and then to obtain the pressure field. A simplified procedure description in SIMPLE [38] is shown below:

1. Solve the Navier-Stokes equation with a guessed pressure field p^*, then we will have its corresponding face flux J_f^*.

2. To satisfy the continuity equation, adding a correction term ${J_f}^c$ to J_f^*.

   $$J_f = J_f^* + {J_f}^c \tag{14}$$

   $${J_f}^c = d_f({p_{c0}}^c - {p_{c1}}^c) \tag{15}$$

   where $p^c$is cell pressure correction, p_{c0} and p_{c1} are the pressure at two sides of an element cell, d_f is controlled by $\bar{a}_P$,the average of the linearized momentum equation coefficients a_P for cells adjacent to the face f.

3. Substitute after-correction equations into continuity equation to get a discrete form pressure correction equation within the cell:

$$a_P p' = \sum_{nb} a_{nb} p'_{nb} + b \quad (16)$$

where b is the net mass flow into cells.

$$\mathrm{b} = \sum_f^{N_{faces}} J_f^* A_f \quad (17)$$

4. After obtaining the solution, corrections are made to the cell pressure and cell face fluxes.

$$p = p^* + \alpha_p p' \quad (18)$$

$$J_f = J_f^* + d_f (p'_{c0} - p^*_{c1}) \quad (19)$$

where α_p is the under-relaxation factor for pressure correction.

Chapter.3 SIMULATION

Numerical simulations of droplet impacting on solid surfaces are performed in ANSYS FLUENT 19.0 in this chapter in order to get the general dependency of droplet impacting behaviors on the initial droplet conditions and surface wettability.

3.1 Simulation Geometry and Boundary Conditions

To study the transient process of droplet impacting onto dry solid surface, a 2D two-phase domains are created in this thesis. For this zero-degree inclined angle (flat bottom surface) case, the bottom length of the inverted T-shaped domain is 16 mm and the height of this whole domain is 3 mm as shown in the figure below. The height of the upper part in this inverted T-shaped domain is 2 mm and its counterpart in the lower part is 1 mm. This inverted T-shaped geometry is chosen to decrease the numerical simulation time.

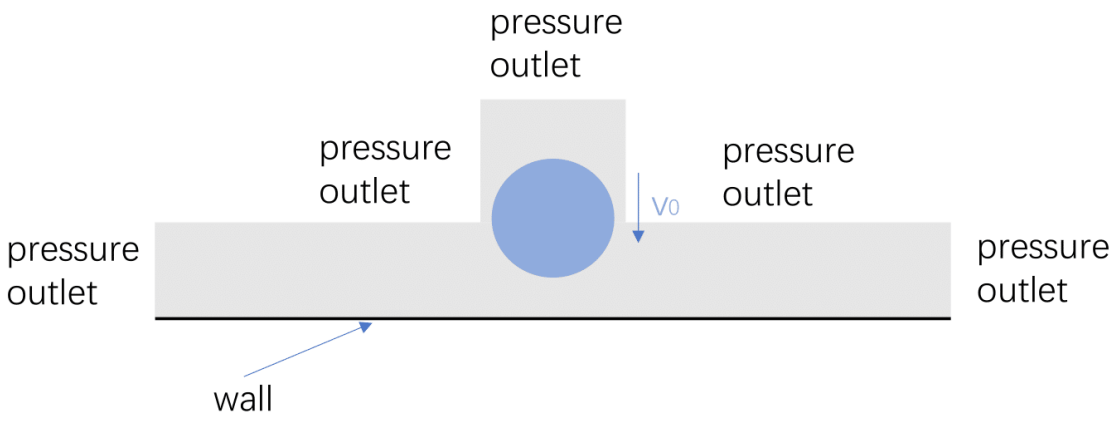

FIGURE3-1. T-shaped domain for droplet impacting simulation with bottom length as 16mm and overall height as 3mm. (-droplet; -air above surface; -bottom surface) Due to the spherical properties of a droplet, the 3D droplet behaviors can be represented in this 2D domain.

All the back pressure at pressure-outlet boundaries are controlled at 1 atm and the ambient temperature is 298 K. The material of the wall boundary is copper with varying surface roughness through different cases and the wall temperature is set to be the same with environment temperature.

3.2 Initialization

In this study, several operating groups with different Weber numbers are tested in 2D flat bottom surface domain. Because it is hard to record all the droplet free falling process from the very beginning in the numerical simulation. In this thesis, initially, a circle with droplet initial diameter d_0 and water volume fraction $\alpha_2 = 1$ will be patched and centered on the axis of symmetry at the height of 1.5 mm above from the bottom surface. The initial droplet diameter d_0 ,impact velocity v_i and initial patched velocity v_0 are shown in the Table 3-1.

Table 3-1. The numerical operating conditions including Weber number, impacting velocity v_i, initial patched velocity v_0 and initial droplet diameter d_0.

	Weber Number	**vi (m/s)**	**v0 (m/s)**	**d (m)**
Group 1	28.75	1.24	1.224075	0.001357
Group 2	59.96	1.85	1.839364	0.001257
Group 3	105.19	2.32	2.311528	0.001412

The initial environment temperature and initial bottom surface temperature are both controlled at 298 K.

3.3 Mesh Independence Test

Three meshes with different element sizes (0.02 mm, 0.03 mm, and 0.035mm) are tested in this section and the meshes details are given in Table 3-2. The minimum size represents the minimum length of grid edges and the max face size means the max length of the edge in a face cell. To capture a more accurate droplet spreading behavior on solid surface, the grids are refined near the bottom wall boundary.

After running simulations under the same operating condition in these three meshes mentioned above, the variation of droplet contact time and droplet maximum spreading area are analyzed and compared in the following figures. Every numerical simulation cases are controlled at the same operating condition. The droplet diameter is set as 1.2 mm, the impacting velocity is 1.85 m/s and the overall Weber number is 54.86.

As shown in FIGURE 3-3, the droplet contact time slightly increases and the droplet peak time (time taken for droplet reaching its maximum spreading area) barely varies. From the information in FIGURE 3-4, the maximum droplet spreading area only changing with the deviation range of 0.463%.

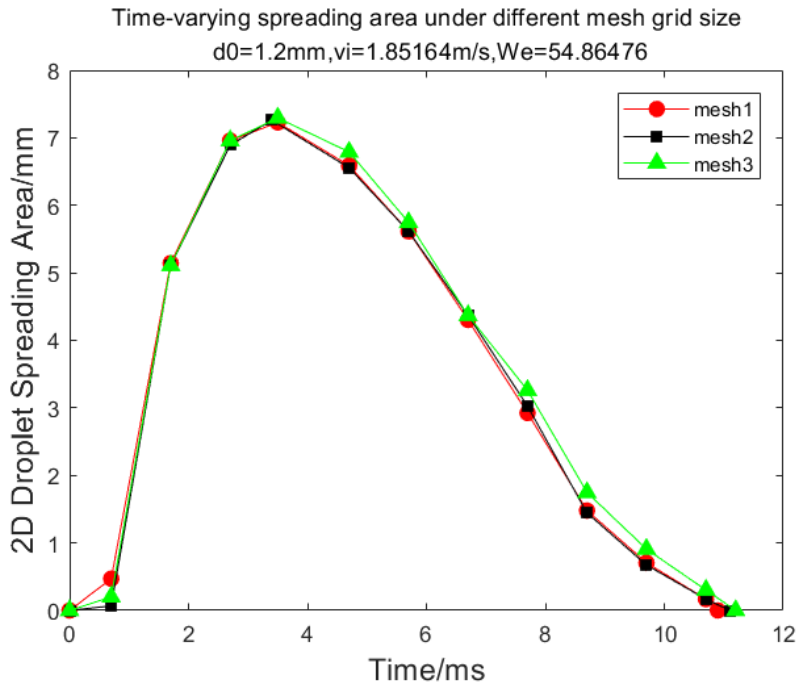

FIGURE3-2. Numerical simulation results of time-varying spreading area under different mesh gird sizes.

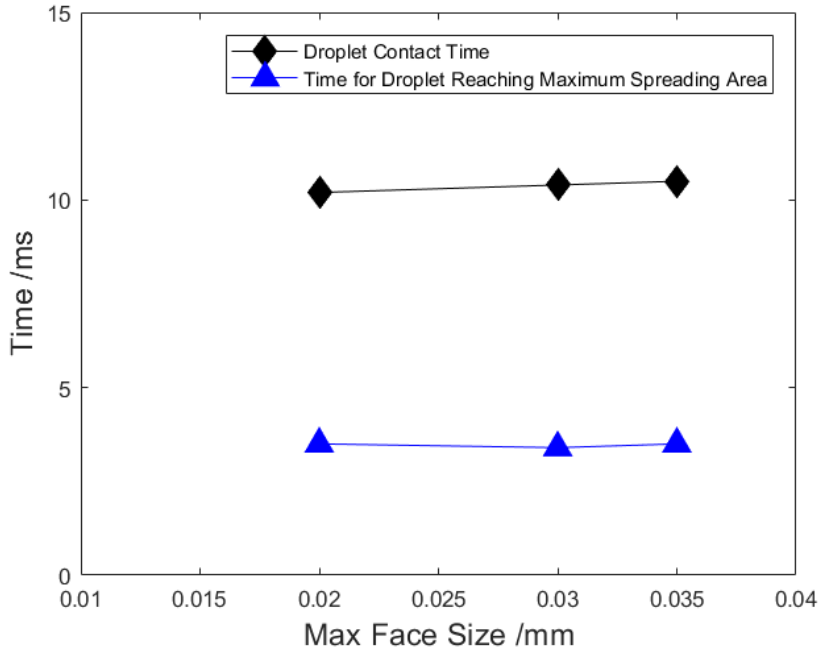

FIGURE3-3. Numerical simulation results of droplet contact time and peak time versus max face size in three different meshes. In these three cases, the max deviation of droplet contact time is 1.61% and the max deviation for peak time is 1.92%.

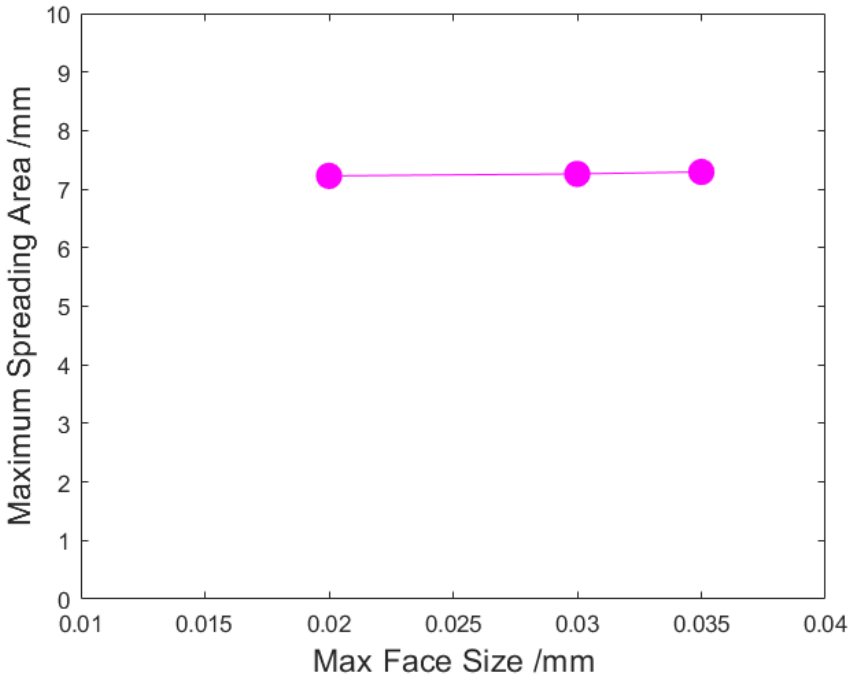

FIGURE3-4. Numerical simulation results of maximum droplet spreading area varying with max face size in different meshes. The max deviation of the maximum spreading area is 0.463%.

Table 3-2. Detail information of three meshes and the results of mesh independent test.

	Max Face Size (mm)	**Number of Elements**	**Droplet Contact Time (ms)**	**Droplet Peak Time (ms)**	**Maximum Spreading Area (mm)**
mesh1	0.035	25234	10.2	3.5	7.2269
mesh2	0.03	33810	10.4	3.4	7.2605
mesh3	0.02	59992	10.5	3.5	7.2941

Chapter.4 RESULTS AND DISCUSSION

In this chapter, the droplet contact time is defined as the time of droplet staying on surface within an impacting process and the droplet peak time is defined as the time for a droplet to reach its maximum spreading area on the bottom surface.

To avoid manual errors and enhance the efficiency and accuracy of every data value, all following 2D droplets spreading area and droplet contact time are measured from droplet impacting video via MATLAB code.

4.1 Effect of Surface Roughness on Droplet Impacting Behavior

In this section, the surface hydrophobicity effect on droplet spreading and rebound behaviors will be evaluated by plotting the contact area versus time under two different surface contact angles $\mathrm{CA} = 120^\circ$ and $\mathrm{CA} = 160^\circ$ and the Weber number value is controlled at 64 for every group. Each group will have two simulation cases with droplet initial diameter $d_0 = 1\ mm$ and $d_0 = 1.2\ mm$.

Inspecting FIGURE 4-1, the droplet maximum contact area increases as the surface roughness decreases and the higher hydrophobicity cases have shorter droplet peak times. The phenomenon above leads to our next analysis topic, the general effect of surface roughness to the maximum droplet contact area.

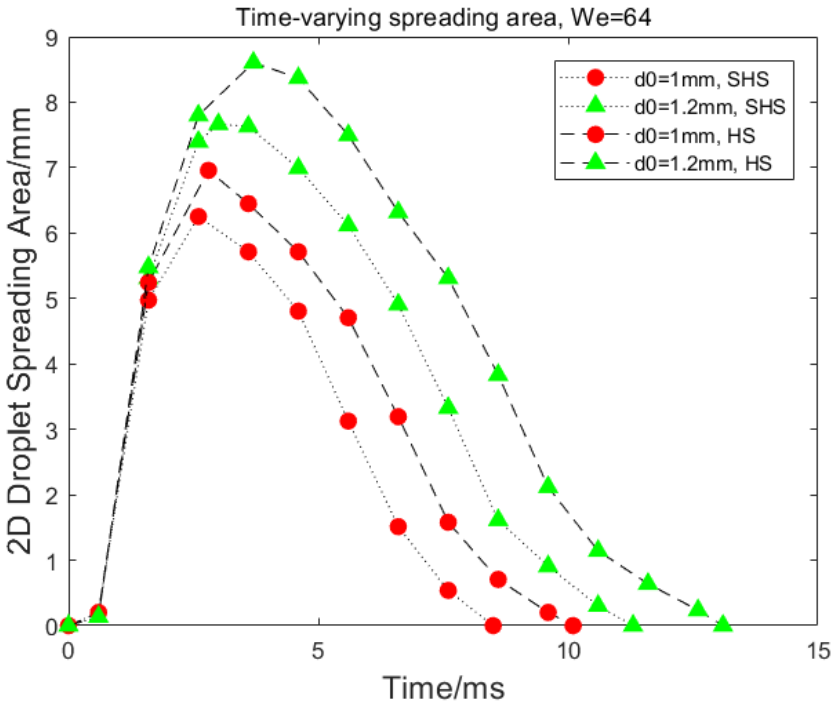

FIGURE4-1. Time-varying spreading contact area while droplet impacting on solid surface with different surface roughness at We=64. HS means the bottom surface contact angle is 120° and SHS means the bottom surface contact angle equals to 160° .

4.2 Effect of Surface Roughness on Droplet Maximum Contact Area

Under room temperature T=298 K, droplet impacting process is simulated at seven different surface roughness conditions ranging from hydrophilic to hydrophobic with contact angles values at 70°, 80°, 90°, 100°, 120°, 140°,160°. The first three cases represent the hydrophilic surface conditions and the transition surface roughness state. Then, the next four cases represent the hydrophobic surface condition among which the 160° case is conventionally defined as superhydrophobic surface.

M. Pasandideh-Fard [12] proposed a simple analytical model to predict the maximum droplet diameter after impact. The maximum spreading factor $\xi_{max} = \frac{D_{max}}{D}$ in his study is given as:

$$\xi_{max} = \frac{D_{max}}{D} = \sqrt{\frac{We+12}{3(1-cos\theta_a)+4(We/\sqrt{Re})}} \quad (20)$$

The contact angle θ_a is assumed to be constant in this model and equals the measured equilibrium contact angle θ_e.

In this section, the effect of surface roughness on the maximum droplet spreading area is assessed by plotting both the numerical and model predictions of normalized maximum spreading area with respect to contact angle under two different Weber numbers, where all impacting situations are the same.

We can interpret from FIGURE 4-2 that the Pasandideh-Fard model can predict the numerical results of both cases with Weber number values at 28.75 and 59.96 at an acceptable accuracy.

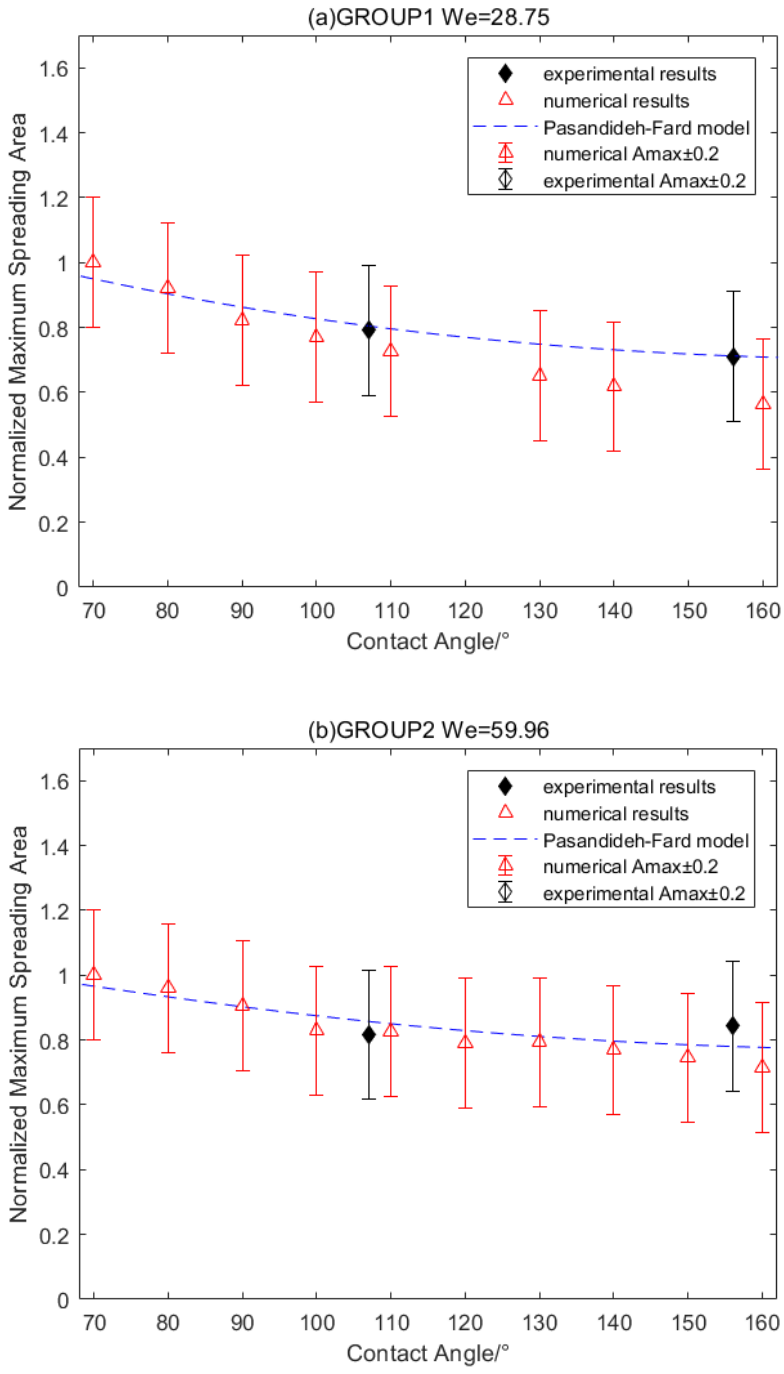

FIGURE4-2. Results of maximum spreading area versus contact angle obtained from numerical simulations, experiments and Pasandideh-Fard model under (a)we=28.75 and (b)we=59.96.

4.3 Effect of Weber Number on Spreading Area via Varying Impact Velocity

In this section, the outcomes of normalized spreading area are investigated under various impacting velocities. The values of Weber numbers are 36, 51.84, and 64, respectively, in the following numerical simulations. To avoid the effect of droplet size on droplet spreading behaviors, the droplet diameter d_0 is set to be 1.2 mm for all simulations.

In FIGURE 4-3, we can see that the numerical results show the same trend as our expectations. Generally, we expect that the droplet spreading area on solid surface will increase first and then decrease after the impact. Due to the higher kinetic energy of droplet for higher impacting velocity cases, the maximum spreading area increases with the Weber number for both surface roughness conditions. Moreover, the time used for droplet reaching its maximum spreading area becomes shorter as the impact velocity increases. However, it can be observed that the droplet contact time are almost the same and the factors that can influence droplet contact time will be discussed in Chapter 4.5.

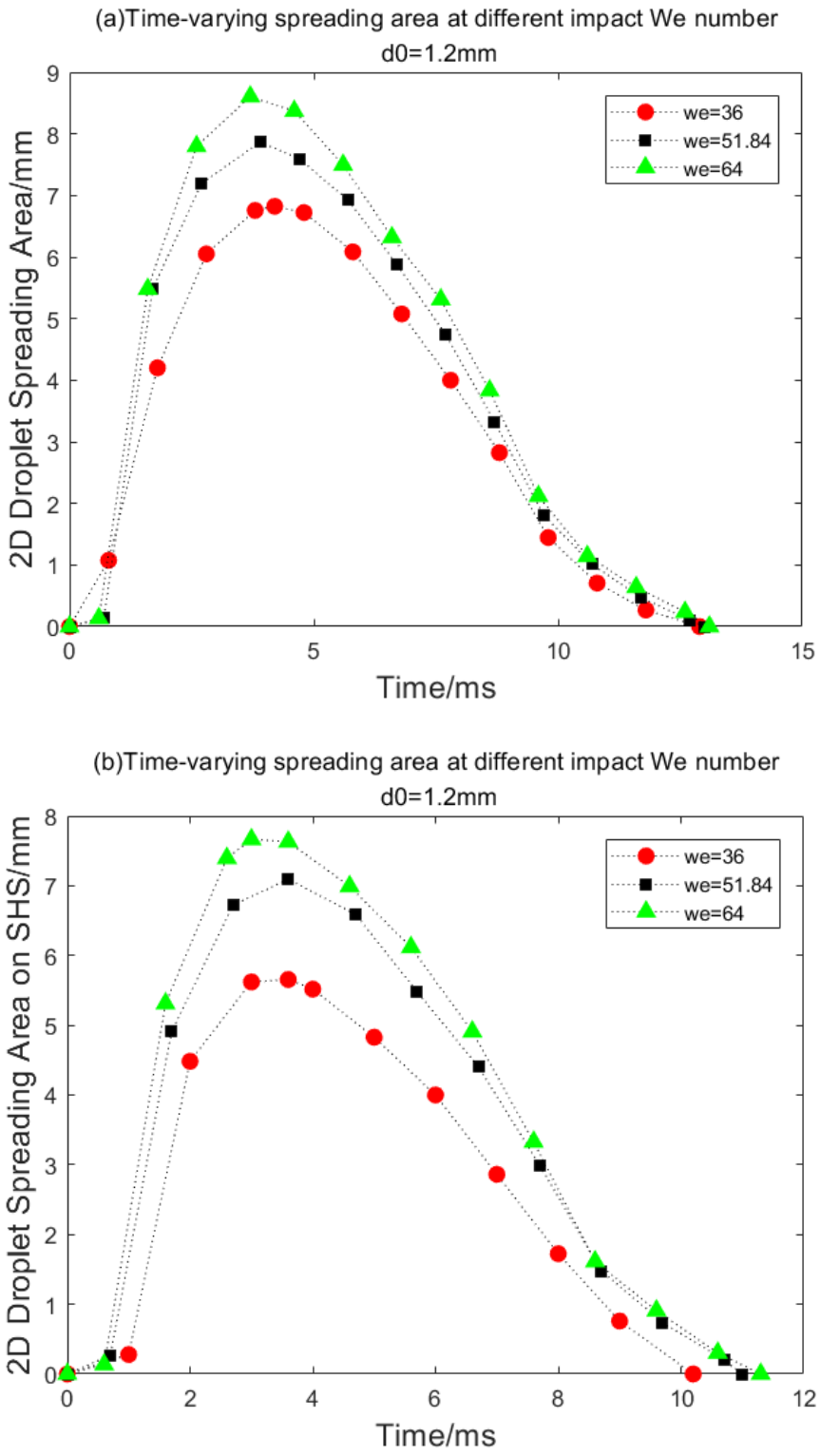

FIGURE4-3. Time-varying spreading area during droplet impacting onto solid surface with droplet diameter equals to 1.2 mm and different droplet impacting velocities values at 1.5 m/s, 1.8 m/s, and 2 m/s when (a) contact angle=120° (b) contact angle=160° .

4.4 Effect of Weber Number on Spreading Area via Varying Initial Droplet Diameter

The time-varying droplet contact area is investigated under different initial droplet diameters and the impacting velocity $v_i = 2\ m/s$ is the same for all simulations. Two kinds of surface roughness, surface contact angles value at 120° and 160°, are considered in this section.

We can see from FIGURE 4-4 that the droplet contact times positively correlate with the initial droplet diameters. Combining the influences of impact velocity on droplet contact time from the outcomes in Chapter 4.3 with those of initial droplet size from the results in this chapter, we can conclude that the droplet contact times are generally independent with the impacting velocities and positively depend on initial droplet sizes. The detailed effects of droplet size on droplet contact time will be evaluated in the next section.

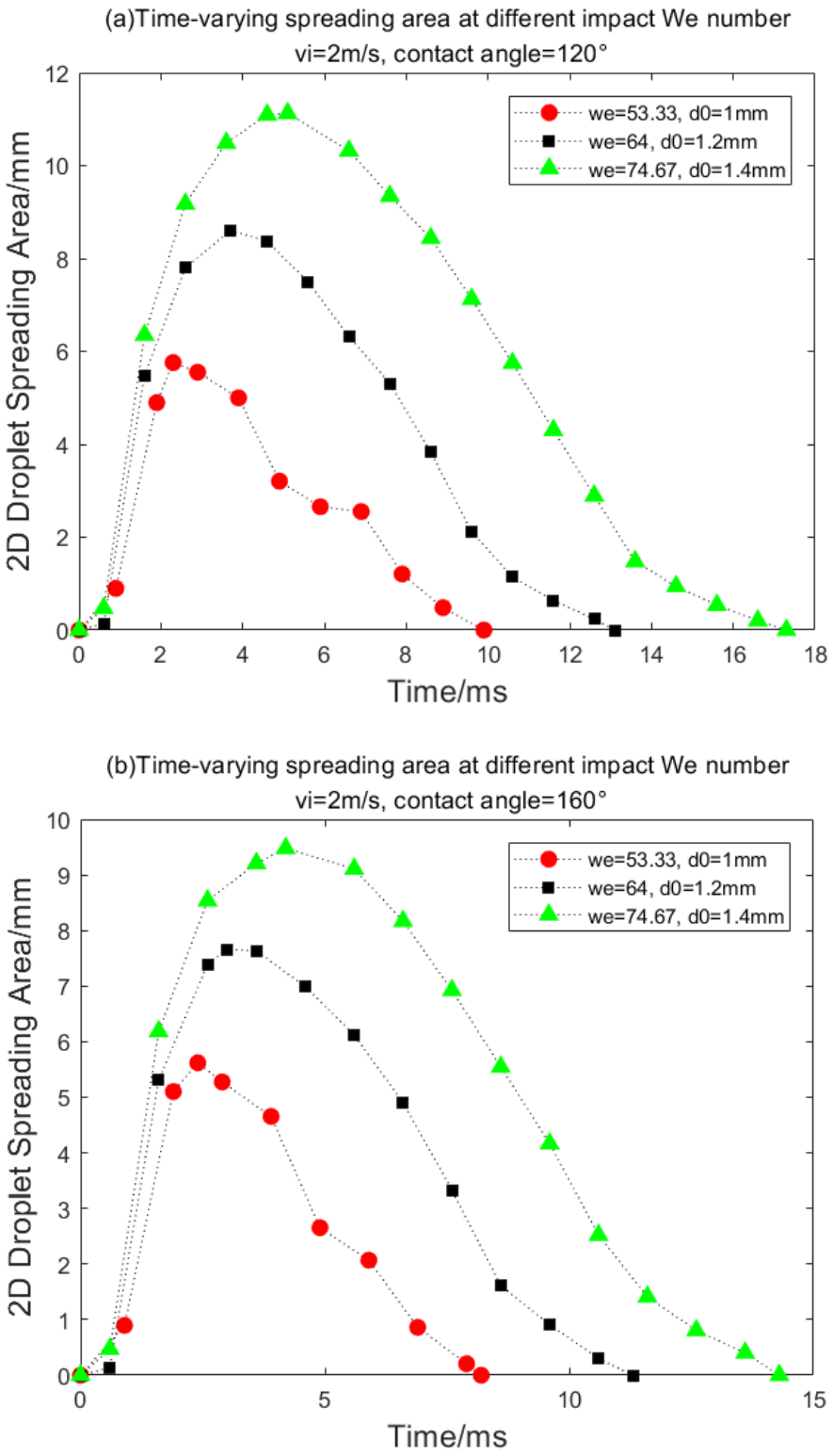

FIGURE4-4. Time-varying spreading contact area while droplet impacting onto solid surface with impacting velocity equals to 2 m/s and different initial droplet diameter values at 53.33, 64, and 74.67 when (a) CA=120° (b)CA=160°

4.5 Effect of Droplet Diameter on Droplet Contact Time

Droplet contact time in this thesis is defined as the time interval from first droplet-solid contact to droplet bouncing back. In previous studies [22], the droplet contact time was found to be the only function of drop mass m and liquid surface tension σ and independent from the impacting velocity v_i. A model proposed by Richard D [23] is given below.

$$t_R = 2.6(\rho D_0^3/8\sigma)^{1/2} \tag{21}$$

In this part, a series of droplet impacting simulations with different droplet diameters values at 0.8 mm, 1.0 mm, 1.2 mm, 1.4 mm, and 1.6 mm are investigated under the same Weber number. The contact time dependency on droplet diameter is evaluated by plotting the normalized contact time in both the numerical results and the theoretical model outcomes.

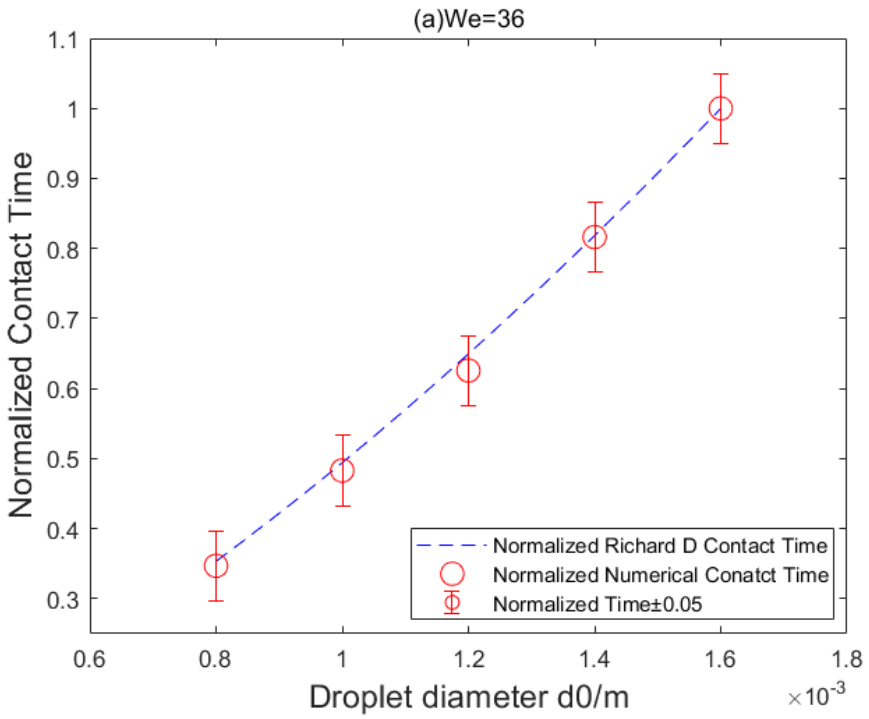

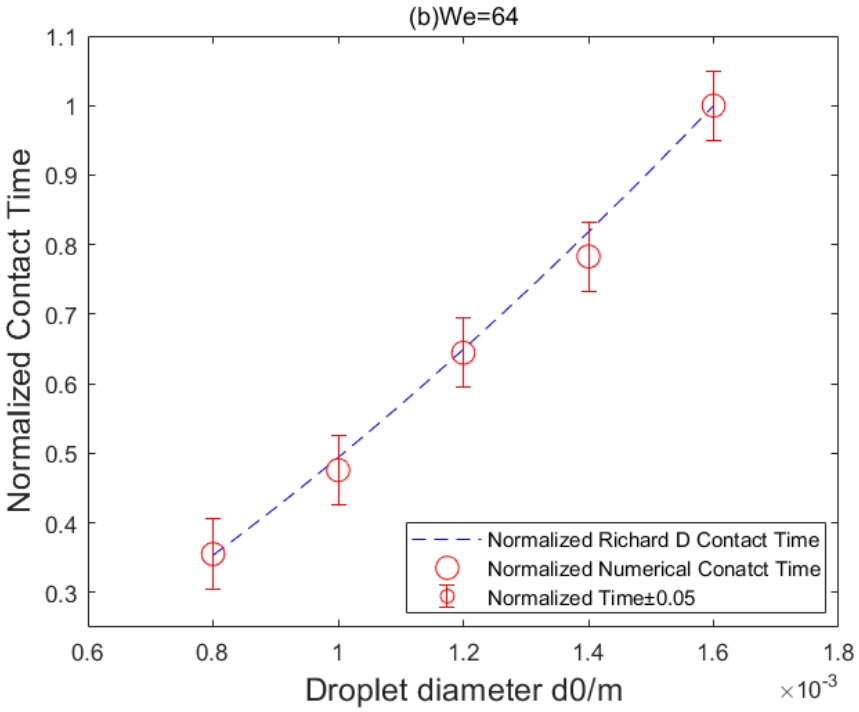

FIGURE4-5. Comparisons between results of normalized droplet contact time versus droplet diameters obtained from numerical results to those of Richard D model under(a)We=36 and (b)We=64.

Chapter.5 DROPLET IMPACTING MEASUREMENT

A droplet impacting experiment is performed to test the droplet spreading and bouncing behaviors under real-life situation. The droplet transient impacting behaviors are captured by High-Speed Camera.

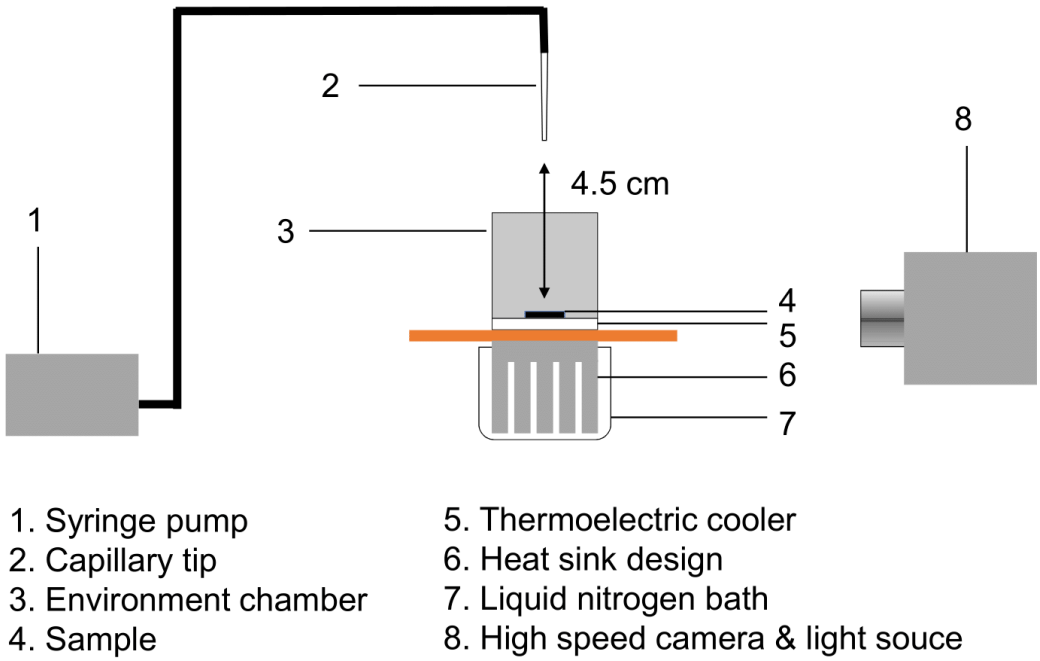

FIGURE5-1. Experiment set-up of droplet impacting.

1. Syringe pump (11 Plus, Harvard Apparatus), used to create a flow rate at 0.3 mL/min.
2. Capillary tip (Kyowa Interface Science), around 1μL droplets will be dispensed from this capillary tip.
3. Environment chamber, used to maintain the environmental temperature and humidity.
4. Sample, three samples with different surface roughness.
5. Thermoelectric cooler, used to create low temperature on sample surface ranging from -15° C to -70° C.
6. Heat sink design, used to maintain the low experimental temperature.
7. Liquid nitrogen bath, used to create low temperature.
8. High speed camera (MiniAX, Photron) and Light source: LED illuminator (Sugar CUBE, USHIO), High speed camera is used to capture the transient process of droplets impacting the surface and the light source is used to create a bright background on camera pictures.

Two groups of droplet impacting tests with different Weber number valuing at 28.75 (case 1) and 59.96 (case 2) are performed in experiments. For case 1, the impacting velocity is 1.24 m/s and the droplet initial diameter is 0.001357 m. For case 2, the impacting velocity is 1.85 m/s and the droplet initial diameter is 0.001257 m. Two different samples are copper flat surface (contact angle=109°) and superhydrophobic surface (contact angle=156°) respectively.

Both samples are tested under each case mentioned above. The time-lapse images captured by High-speed camera are represented in FUGURE 6-2 below.

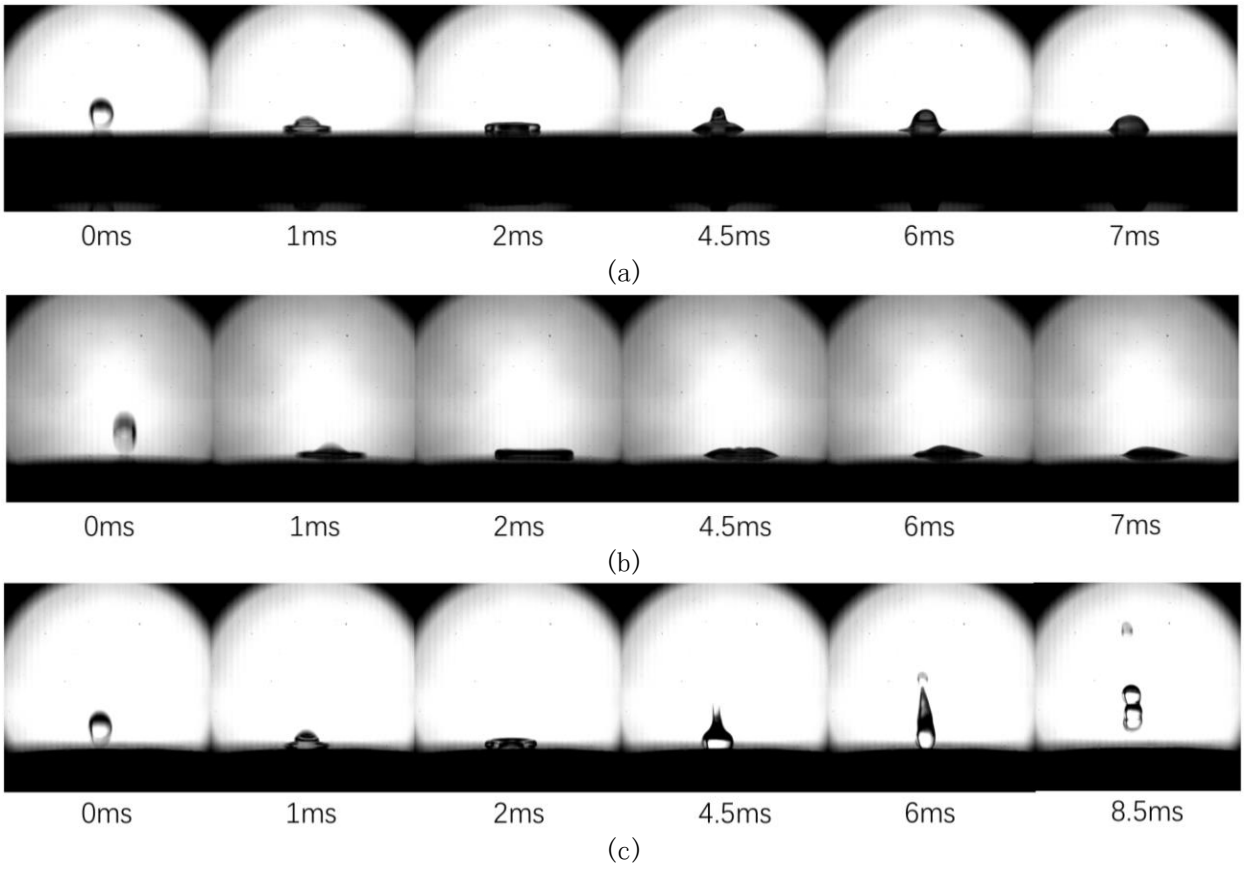

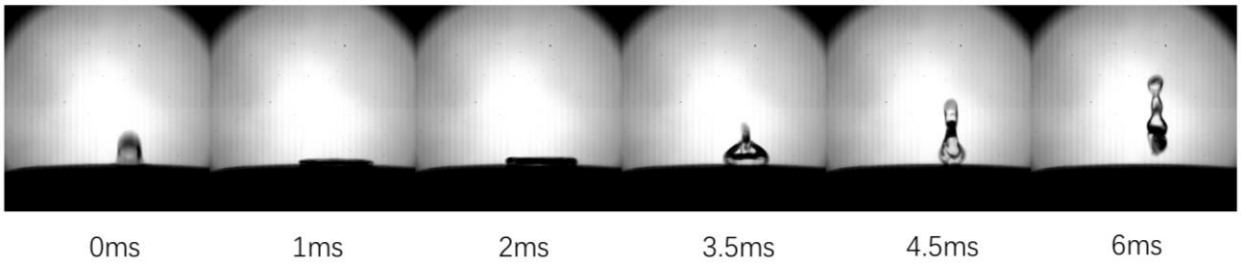

(d)

FIGURE5-2. Time-lapsed images of droplet impacting behavior captured by High-speed camera under different impact conditions and surface roughness situations
(a) Copper flat surface, case 1 (b) Copper flat surface, case 2
(c) Superhydrophobic surface, case 1 (d) Superhydrophobic surface, case 2

The experimental results of normalized maximum droplet spreading areas are compared with both the numerical results and the theoretical model in FIGURE 4-2.

Chapter.6 SUMMARY

Numerical, experimental, and theoretical approaches are harnessed to investigate the phenomenon of droplet impacting on flat solid surface in this thesis. Based on FLUENT 19.0, a series of numerical simulations are performed to analyze the spreading and bouncing behaviors in droplet impacting process. The effects of various parameters upon droplet impacting behaviors are explored.

The controlling variables including bottom surface roughness, droplet impacting velocity, initial droplet diameter and impacting Weber number are varied to investigate their effects on droplet spreading and bouncing back behaviors. Especially, for the bottom surface with contact angle at 160° (conventionally defined as superhydrophobic surface), outcomes show that the numerical and experimental results of normalized droplet contact time are comparable with the theoretical model predictions. Moreover, the time-varying spreading area is examined under different impacting Weber numbers. The results show that the maximum spreading area will increase as the impacting Weber number increases and the peak time will be shorter for higher impacting Weber number. In general, the maximum droplet spreading area positively relates to the increase of droplet diameter and droplet impacting velocity and negatively correlates to the increase of surface roughness and the surface tension. For droplets with similar droplet mass, the droplet contact time are independent of Weber number. The droplet contact time is the only function of droplet physics properties and it shows in this thesis that the droplet contact time will increase as the droplet size increases.

Reference

[1]. Antonini C, Villa F, Marengo M. Oblique impacts of water drops onto hydrophobic and superhydrophobic surfaces: outcomes, timing, and rebound maps. Experiments in fluids, 2014, 55(4): 1713.

[2]. McKinley G H, Renardy M. Wolfgang von ohnesorge. Physics of Fluids, 2011, 23(12): 127101.

[3]. Richard D, Clanet C, Quéré D. Surface phenomena: Contact time of a bouncing drop. Nature, 2002, 417(6891): 811.

[4]. Šikalo Š, Wilhelm H D, Roisman I V, et al. Dynamic contact angle of spreading droplets: Experiments and simulations. Physics of Fluids, 2005, 17(6): 062103.

[5]. Yarin A L. Drop impact dynamics: splashing, spreading, receding, bouncing…. Annu. Rev. Fluid Mech., 2006, 38: 159-192.

[6]. Khojasteh D, Kazerooni M, Salarian S, et al. Droplet impact on superhydrophobic surfaces: A review of recent developments. Journal of Industrial and Engineering Chemistry, 2016, 42: 1-14.

[7]. Marengo M, Antonini C, Roisman I V, et al. Drop collisions with simple and complex surfaces. Current Opinion in Colloid & Interface Science, 2011, 16(4): 292-302.

[8]. LeClear S, LeClear J, Park K C, et al. Drop impact on inclined superhydrophobic surfaces. Journal of colloid and interface science, 2016, 461: 114-121.

[9]. Michel T, Mock U, Roisman I V, et al. The hydrodynamics of drop impact onto chemically structured surfaces. Journal of Physics: Condensed Matter, 2005, 17(9): S607.

[10]. Antonini C, Villa F, Marengo M. Oblique impacts of water drops onto hydrophobic and superhydrophobic surfaces: outcomes, timing, and rebound maps. Experiments in fluids, 2014, 55(4): 1713.

[11]. Jin Z, Sui D, Yang Z. The impact, freezing, and melting processes of a water droplet on an inclined cold surface. International journal of heat and mass transfer, 2015, 90: 439-453.

[12]. Pasandideh‐Fard M, Qiao Y M, Chandra S, et al. Capillary effects during droplet impact on a solid surface. Physics of fluids, 1996, 8(3): 650-659.

[13]. Chen L, Xiao Z, Chan P C H, et al. A comparative study of droplet impact dynamics on a dual-scaled superhydrophobic surface and lotus leaf. Applied surface science, 2011, 257(21): 8857-8863.

[14]. Malgarinos I, Nikolopoulos N, Marengo M, et al. VOF simulations of the contact angle dynamics during the drop spreading: standard models and a new wetting force model. Advances in colloid and interface science, 2014, 212: 1-20.

[15]. Yang X, Ray M, Kong S C, et al. SPH simulation of fuel drop impact on heated surfaces. Proceedings of the Combustion Institute, 2019, 37(3): 3279-3286.

[16]. Peng D Y, Robinson D B. A new two-constant equation of state. Industrial & Engineering Chemistry Fundamentals, 1976, 15(1): 59-64.

[17]. Liu C, Zhu L, Bu W, et al. Superhydrophobic surfaces: From nature to biomimetic through VOF simulation. Micron, 2018, 107: 94-100.

[18]. Dupont J B, Legendre D. Numerical simulation of static and sliding drop with contact angle hysteresis. Journal of Computational Physics, 2010, 229(7): 2453-2478.

[19]. Li D, Duan X. Numerical analysis of droplet impact and heat transfer on an inclined wet surface. International Journal of Heat and Mass Transfer, 2019, 128: 459-468.

[20]. Zhu Y, Liu H R, Mu K, et al. Dynamics of drop impact onto a solid sphere: spreading and retraction. Journal of Fluid Mechanics, 2017, 824.

[21]. Bordbar A, Taassob A, Khojasteh D, et al. Maximum Spreading and Rebound of a Droplet Impacting onto a Spherical Surface at low Weber numbers. Langmuir, 2018, 34(17): 5149-5158.

[22]. Clanet C, Béguin C, Richard D, et al. Maximal deformation of an impacting drop. Journal of Fluid Mechanics, 2004, 517: 199-208.

[23]. Richard D, Clanet C, Quéré D. Surface phenomena: Contact time of a bouncing drop. Nature, 2002, 417(6891): 811.

[24]. Levin Z, Hobbs P V. Splashing of water drops on solid and wetted surfaces: hydrodynamics and charge separation. Philosophical Transactions of the Royal Society of London. Series A, Mathematical and Physical Sciences, 1971, 269(1200): 555-585.

[25]. Hung L S, Yao S C. Experimental investigation of the impaction of water droplets on cylindrical objects. International journal of multiphase flow, 1999, 25(8): 1545-1559.

[26]. Wang Z, Lopez C, Hirsa A, et al. Impact dynamics and rebound of water droplets on superhydrophobic carbon nanotube arrays. Applied physics letters, 2007, 91(2): 023105.

[27]. Range K, Feuillebois F. Influence of surface roughness on liquid drop impact. Journal of colloid and interface science, 1998, 203(1): 16-30.

[28]. Rein M. Phenomena of liquid drop impact on solid and liquid surfaces. Fluid Dynamics Research, 1993, 12(2): 61.

[29]. Mao T, Kuhn D C S, Tran H. Spread and rebound of liquid droplets upon impact on flat surfaces. AIChE Journal, 1997, 43(9): 2169-2179.

[30]. Mao T, Kuhn D C S, Tran H. Spread and rebound of liquid droplets upon impact on flat surfaces. AIChE Journal, 1997, 43(9): 2169-2179.

[31]. Biance A L, Clanet C, Quéré D. First steps in the spreading of a liquid droplet. Physical Review E, 2004, 69(1): 016301.

[32]. Clanet C, Béguin C, Richard D, et al. Maximal deformation of an impacting drop. Journal of Fluid Mechanics, 2004, 517: 199-208.

[33]. Fedorchenko A I, Wang A B. On some common features of drop impact on liquid surfaces. Physics of Fluids, 2004, 16(5): 1349-1365.

[34]. Fukai J, Zhao Z, Poulikakos D, et al. Modeling of the deformation of a liquid droplet impinging upon a flat surface. Physics of Fluids A: Fluid Dynamics, 1993, 5(11): 2588-2599.

[35]. He G, Hadjiconstantinou N G. A molecular view of Tanner's law: molecular dynamics simulations of droplet spreading. Journal of Fluid Mechanics, 2003, 497: 123-132.

[36]. Mundo C H R, Sommerfeld M, Tropea C. Droplet-wall collisions: experimental studies of the deformation and breakup process. International journal of multiphase flow, 1995, 21(2): 151-173.

[37]. Okumura K, Chevy F, Richard D, et al. Water spring: A model for bouncing drops. EPL (Europhysics Letters), 2003, 62(2): 237.

[38]. ANSYS FLUENT 12.0 User’s Guide. Release 12.0 © ANSYS, Inc. 2009-01-29

[39]. Brandt A. Multi-level adaptive computations in fluid dynamics[C]//4th Computational Fluid Dynamics Conference. 1979: 1455.

[40]. Cho S C, Wang Y, Chen K S. Droplet dynamics in a polymer electrolyte fuel cell gas flow channel: Forces, deformation, and detachment. I: Theoretical and numerical analyses. Journal of power sources, 2012, 206: 119-128.

[41]. Cho S C, Wang Y, Chen K S. Droplet dynamics in a polymer electrolyte fuel cell gas flow channel: Forces, Deformation and detachment. II: Comparisons of analytical solution with numerical and experimental results. Journal of Power Sources, 2012, 210: 191-197.

[42]. Moon J H, Kim D Y, Lee S H. Spreading and receding characteristics of a non-Newtonian droplet impinging on a heated surface. Experimental Thermal and Fluid Science, 2014, 57: 94-101.

[43]. Foister R T. The kinetics of displacement wetting in liquid/liquid/solid systems. Journal of colloid and interface science, 1990, 136(1): 266-282.

[44]. Cazabat A M, Valignat M P, Villette S, et al. The mechanism of spreading: a microscopic description. Langmuir, 1997, 13(17): 4754-4757.

[45]. Dussan E B. On the spreading of liquids on solid surfaces: static and dynamic contact lines. Annual Review of Fluid Mechanics, 1979, 11(1): 371-400.

[46]. De Gennes P G. Wetting: statics and dynamics. Reviews of modern physics, 1985, 57(3): 827.

[47]. Kavehpour H P. An interferometric study of spreading liquid films. Massachusetts Institute of Technology, 2003.

[48]. Worthington AM. 1908. A Study of Splashes. London: Longmans, Green. 129 pp.